Article:
Díaz, J.S. and Rigby, S.E. (2022) Blast wave kinematics: theory, experiments, and applications. Shock Waves, 32 (5). pp. 405-415. ISSN: 0938-1287

https://doi.org/10.1007/s00193-022-01089-z

Shock Waves (2022) 32:405–415
https://doi.org/10.1007/s00193-022-01089-z

ORIGINAL ARTICLE

Blast wave kinematics: theory, experiments, and applications

J. S. Díaz[1] · S. E. Rigby[2]

Received: 20 October 2021 / Revised: 1 June 2022 / Accepted: 13 June 2022 / Published online: 25 July 2022

Abstract
Measurements of the time of arrival of shock waves from explosions can serve as powerful markers of the evolution of the shock front for determining crucial parameters driving the blast. Using standard theoretical tools and a simple ansatz for solving the hydrodynamics equations, a general expression for the Mach number of the shock front is derived. Dimensionless coordinates are introduced allowing a straightforward visualization and direct comparison of blast waves produced by a variety of explosions, including chemical, nuclear, and laser-induced plasmas. The results are validated by determining the yield of a wide range of explosions, using data from gram-size charges to thermonuclear tests.

Keywords Blast · Sedov–Taylor–von Neumann · Strong shock · Time of arrival · Yield estimation

List of symbols

a_0	Speed of sound in undisturbed air
E_m	Specific energy per unit mass
E_0	Blast energy
f	Dimensionless pressure
K	Dimensionless energy
K_0	Dimensionless energy in the strong-shock regime
K_1	Dimensionless energy in the far field
M_S	Mach number
P	Pressure
P_0	Atmospheric pressure
ΔP	Peak hydrostatic overpressure
r	Radial coordinate
R	Shock front radius
R_0	Characteristic explosion length
t	Time
u	Particle radial velocity
W	Explosive mass
z	Dimensionless scaled shock radius
z_low	Lower value for range of strong-shock validity
z_upp	Upper value for range of strong-shock validity
Z	Scaled distance (cube-root scaling)
γ	Heat capacity ratio
η	Dimensionless radial coordinate
κ_i	Auxiliary exponents of hydrodynamic functions in the strong-shock regime ($i = 1, \ldots, 4$)
λ	Dimensionless inverse squared Mach number
ϕ	Dimensionless particle speed
ψ	Dimensionless density
ρ	Density
ρ_0	Atmospheric density
τ	Dimensionless scaled time
ζ	Jacobian factor

Communicated by M. Hargather.

✉ S. E. Rigby
sam.rigby@sheffield.ac.uk

J. S. Díaz
jsdiazpo@iu.edu

[1] Physics Department, Indiana University, Bloomington, IN 47405, USA

[2] Department of Civil and Structural Engineering, University of Sheffield, Mappin Street, Sheffield S1 3JD, UK

1 Introduction

Recent large-scale industrial accidents such as those in Tianjin (2015; 173 deaths) and Beirut (2020; 218 deaths) provide stark illustrations of the devastating potential of explosions. In addition to the tragic loss of human lives, the latter caused an estimated $15B in property damage: complete destruction of buildings extended to a few hundred metres from the source of the explosion, and broken glass and debris was observed at distances up to 3 km from the explosion center, encompassing an area with more than 750,000 inhabitants [1]. Clearly, in order for engineers to design structures for resilience against explosions, the properties of the blast wave

must be known both relatively close to (where the structure should be designed to avoid/limit progressive and disproportionate collapse) and relatively far from the source (where the majority of injuries are caused by either lacerations from airborne glass fragments or by damage to hearing from failed glass panels [2]).

Knowledge of the arrival time of a blast wave at various distances from the source enables a radius–time relationship to be developed, from which other key parameters such as peak pressure can be derived [3–5]. Thus, the ability to determine this relationship a priori, from a known explosive yield, will provide vital information on the properties of the blast wave as it propagates. Further, a well-defined relationship that is valid for any distance permits the yield of an explosive to be determined through inverse analysis [6].

Theoretical studies of blast wave physics date back to the first half of the last century. Some of the most widely known works correspond to the early studies of intense explosions by Taylor [7], von Neumann [9], and Sedov [8]; and further characterizations of the fireball and blast wave solutions in different environments and explosive charge geometries can be found in the literature [4,10–15].

This article presents a description of the propagation of a shock wave produced by an explosion in free air, an extension of the standard strong-shock solution to its later phase transitioning into an acoustic wave, and the applications of the results for estimating the yield of a wide variety of explosions.

2 Theoretical description of the blast wave

Let us model the shock wave produced by an explosion in free air as a sphere of time-dependent radius R.

Let us call E_0 the energy released in the explosion that is transferred to the surrounding air producing the shock wave. For simplicity, the energy release is assumed to occur instantaneously and the air is characterized by undisturbed ambient conditions of atmospheric pressure P_0 and density ρ_0. Conservation of energy and the equation of state of an ideal gas can be used to write the blast energy in the form [3–5,12,13]

$$E_0 = 4\pi \int_0^R \left(\frac{1}{2}\rho u^2 + \frac{P - P_0}{\gamma - 1} \right) r^2 \mathrm{d}r, \tag{1}$$

where r represents a radial coordinate measuring the distance from the center of the explosion to the shock front R. The first integrand represents the kinetic energy density of the gas, whereas the second term corresponds to the thermal energy of the gas contained within a radius R. The factor γ is the heat capacity ratio, assumed to be unaffected by the passing of the shock; its value for air in normal conditions described as a diatomic gas is $\gamma = 1.4$. The radial particle velocity u, pressure P, and density ρ of the air behind the shock front satisfy well-known hydrodynamics equations, which must be solved to determine their radial dependence before performing the integration in (1). Since the integration over the radial coordinate starts from zero, it is important to emphasize that a point source for the energy E_0 has been assumed.

The system of partial differential equations describing the motion, continuity, and equation of state of the fluid are, respectively, given by [3–5,12,13]

$$\frac{\partial u}{\partial t} + u\frac{\partial u}{\partial r} = -\frac{1}{\rho}\frac{\partial P}{\partial r}, \tag{2}$$

$$\frac{\partial \rho}{\partial t} + u\frac{\partial \rho}{\partial r} + \rho\left(\frac{\partial u}{\partial r} + \frac{2u}{r} \right) = 0, \tag{3}$$

$$\left(\frac{\partial}{\partial t} + u\frac{\partial}{\partial r} \right)\left(P\rho^{-\gamma} \right) = 0, \tag{4}$$

subject to the boundary conditions at the shock front given by the Rankine–Hugoniot relations. In terms of the Mach number of shock front $M_S = a_0^{-1}\frac{\mathrm{d}R}{\mathrm{d}t}$, these relations are [3–5,12,13]

$$u(R) = \frac{2a_0 M_S}{\gamma + 1}\left(1 - M_S^{-2}\right), \tag{5}$$

$$\rho(R) = \frac{(\gamma + 1)\rho_0}{\gamma - 1 + 2M_S^{-2}}, \tag{6}$$

$$P(R) = \left(\frac{2\gamma M_S^2 - (\gamma - 1)}{\gamma + 1} \right) P_0, \tag{7}$$

where $a_0 = \sqrt{\gamma P_0/\rho_0}$ is the speed of sound at ambient conditions.

Let us characterize the motion of the shock front by introducing the dimensionless variables

$$\eta = \frac{r}{R}, \quad \lambda = M_S^{-2}, \tag{8}$$

where η specifies the distance from the explosion center ($\eta = 0$) to the shock front ($\eta = 1$), whereas λ characterizes the speed of the shock front from high Mach number ($\lambda \to 0$) to the ambient speed of sound ($\lambda = 1$). Let us now write the ratios of the three quantities of interest in terms of the new variables as

$$\frac{u}{a_0 M_S} = \phi(\eta, \lambda), \quad \frac{\rho}{\rho_0} = \psi(\eta, \lambda), \quad \frac{P}{P_0} = \frac{f(\eta, \lambda)}{\lambda}. \tag{9}$$

The notation for the dimensionless functions has been chosen so that in the strong-shock regime ($M_S \gg 1$) the definitions introduced by Taylor [7] are recovered. Also following Taylor's notation, we have isolated the asymptotically divergent part of the pressure ratio in the strong-shock limit

($\lambda \to 0$) discussed in more detail in Sect. 3. Using the functions (9), the energy equation (1) can be rewritten as

$$z^{-3} + K_1 = \lambda^{-1} K(\lambda), \tag{10}$$

where we have introduced the dimensionless scaled distance $z = R/R_0$, which measures distance in units of the explosion characteristic length $R_0 = (E_0/P_0)^{1/3}$ [16]. Notice that z differs from the standard scaled distance $Z = R/W^{1/3}$ used in blast engineering; the latter normalizes the distance by the cube root of the mass W of the explosive charge, whereas z removes cumbersome units and, more importantly, eliminates sometimes problematic TNT equivalence of different explosive materials. The function $K(\lambda)$ is defined as

$$K(\lambda) = 4\pi \int_0^1 \left(\frac{\gamma}{2} \psi(\eta, \lambda) \phi^2(\eta, \lambda) + \frac{f(\eta, \lambda)}{\gamma - 1} \right) \eta^2 \mathrm{d}\eta. \tag{11}$$

In the limit $R \to \infty$, the blast wave decays to an acoustic wave ($\lambda \to 1$), hence the constant $K_1 \equiv K(1)$ in (10) corresponds to the boundary value of K in the far field. The Jacobian of the coordinate transformation $(r, t) \to (\eta, \lambda)$ produces a term proportional to $\frac{\mathrm{d}\lambda}{\mathrm{d}R}$ that parametrizes the decay of the blast wave. This term appears several times in the hydrodynamic equations and the notation gets simplified by introducing the Jacobian term

$$\zeta(\lambda) = \frac{R}{3\lambda} \frac{\mathrm{d}\lambda}{\mathrm{d}R} = -\frac{2R}{3M_\mathrm{S}} \frac{\mathrm{d}M_\mathrm{S}}{\mathrm{d}R}. \tag{12}$$

In the last expression, the definition (8) has been used; this shows that the Jacobian factor describes how the speed of the shock front decreases as it moves away from the explosion center. From the energy equation (10), it follows that the Jacobian term (12) and $K(\lambda)$ are related by the ordinary differential equation

$$K - \lambda K_1 = \zeta(\lambda) \left(K - \lambda \frac{\mathrm{d}K}{\mathrm{d}\lambda} \right). \tag{13}$$

This relation implies that the Jacobian term must satisfy the boundary conditions $\zeta(0) = 1, \zeta(1) = 0$. Up to this point, we have only made use of standard equations, introduced useful coordinates, and declared definitions to derive and expand well-known results from the blast wave literature. The last two differential equations are obtained, which must be simultaneously satisfied, and commonly numerical methods are introduced for their solution. Nonetheless, in an attempt to go one step further and derive an analytical expression for the Mach number M_S we propose an ansatz for the Jacobian factor. The simplest description of the blast decay that allows for an analytical description of the Mach number of the shock front and satisfies the boundary conditions is the linear decay $\zeta(\lambda) = 1 - \lambda$. Numerical analysis and experimental observations suggest that the decay is nonlinear, with the Mach number decaying more rapidly at early times. In this work, we intend to provide an approximate description of the phenomena; therefore, the linear choice will suffice. Since the boundary conditions are satisfied, our approximate description will match the exact solutions in the early and late regimes, whereas some small deviation can appear in the mid-range where the strong shock transitions to the acoustic wave. In Sect. 4, we will see that the linear ansatz provides a sufficiently accurate descriptions of the blast wave for all ranges.

The linear form of the Jacobian term $\zeta(\lambda)$ leads to a simple solution of (13) given by

$$K(\lambda) = (1 - \lambda) K_0 + \lambda K_1, \tag{14}$$

where the integration constant has been chosen so that K_0 denotes $K(\lambda)$ evaluated at $\lambda = 0$. This solution allows inverting the energy equation (10) to write the Mach number in terms of the scaled distance as

$$M_\mathrm{S}(z) = \frac{\mathrm{d}z}{\mathrm{d}\tau} = \left(1 + \frac{1}{K_0 z^3} \right)^{1/2}, \tag{15}$$

where we have introduced the dimensionless scaled time $\tau = a_0 t/R_0$ [16]. Another reason for using these dimensionless variables (τ, z) is that they allow direct comparison of a wide range of experiments independent of the yield of the explosion under consideration. This enables us to visualize the results from gram-sized charges to megaton yields from thermonuclear explosions in the same plot, as is done in this article. Notice that the definition of λ in (8), the Jacobian term (12), and its linear form can also be used to write a nonlinear differential equation for $M_\mathrm{S}(z)$ in the form $\frac{\mathrm{d}M_\mathrm{S}}{\mathrm{d}R} + \frac{3M_\mathrm{S}}{2R} = \frac{3}{2RM_\mathrm{S}}$. This equation is of the Bernoulli type so that it can be analytically solved; its solution is again given by (15), which confirms the mathematical self-consistency of the system. A Bernoulli differential equation has the form $y' + p(x)y = q(x)y^\alpha$ for a real valued α. The substitution $w = y^{1-\alpha}$ reduces the equation to the linear differential equation $w' + (1 - \alpha)p(x)w = (1 - \alpha)q(x)$ that can be easily solved using standard methods. In the case above, we find $p(R) = q(R) = \frac{3}{2R}$ and $\alpha = -1$.

The solution for the Mach number (15) shows that only the numerical value of the function $K(\lambda)$ (11) at $\lambda = 0$ is needed for fully describing the propagation of the shock front. This observation in turn implies that the solutions of the hydrodynamics functions $\phi(\eta, \lambda)$, $\psi(\eta, \lambda)$, and $f(\eta, \lambda)$ are necessary only at $\lambda = 0$, which significantly simplifies the system of ordinary differential equations (2–4). Using the definitions (9), the solution to the system (2–4) with boundary conditions given by the Rankine–Hugoniot relations (5–7) at $\lambda = 0$ is

$$\phi(\eta,0)=\frac{\eta}{\gamma}+\left(\frac{\gamma-1}{\gamma^2+\gamma}\right)\eta^{\kappa_1}, \tag{16}$$

$$\psi(\eta,0)=\left(\frac{\gamma+1}{\gamma-1}\right)\frac{\eta^{\kappa_2}}{\gamma^{\kappa_3}}\left(\gamma+1-\eta^{\kappa_1-1}\right)^{\kappa_3}, \tag{17}$$

$$f(\eta,0)=\left(\frac{2\gamma^{1-\kappa_4}}{\gamma+1}\right)\left(\gamma+1-\eta^{\kappa_1-1}\right)^{\kappa_4}, \tag{18}$$

where the exponents κ_i, $i=1,\ldots,4$ are only functions of the heat capacity ratio γ:

$$\kappa_1=\frac{7\gamma-1}{\gamma^2-1},\quad \kappa_2=\frac{3}{\gamma-1},\quad \kappa_3=\frac{2\gamma+10}{\gamma-7},$$
$$\kappa_4=\frac{2\gamma^2+7\gamma-3}{\gamma-7}. \tag{19}$$

The three functions in terms of the dimensionless radial coordinate are shown in Fig. 1. We can now use these solutions in the definition of $K(\lambda)$ to determine K_0 in the form

$$K_0=4\pi\int_0^1\left(\frac{\gamma}{2}\psi(\eta,0)\phi^2(\eta,0)+\frac{f(\eta,0)}{\gamma-1}\right)\eta^2\mathrm{d}\eta$$
$$=7.86, \tag{20}$$

where the heat capacity ratio for air has been used since we have assumed the explosion to take place in free air. Once this value is determined, the Mach-number equation (15) can be used to describe the growth of the spherical shock front as a function of the distance from the explosion center. The structure of (15) does not accept an analytical solution and a numerical integration is required; however, it must be noted that (15) is a first-order differential equation that can be trivially solved via computational methods. The numerical solution accompanies this article as Supplementary Material and it is shown in Fig. 2 together with the strong-shock solution discussed in Sect. 3 and the acoustic wave that the general solution must asymptotically approach. We emphasize that (15) represents the key result presented in this article. Instead of using piece-wise semi-empirical definitions, we have obtained an analytical expression for the speed of the shock front that, as shown in Fig. 2, smoothly transitions from the strong-shock solution into the acoustic regime. The continuous decay of the Mach number is displayed in bottom panel of Fig. 2, that approaches $M_S\to 1$ as the numerical solution of (15) evolves from an intense explosion to an acoustic wave. This equation is obtained from conservation of energy (1), which requires the evaluation of the solutions for u, P, and ρ inside the shock front using the Rankine–Hugoniot relations as boundary conditions for solving the hydrodynamic equations (2–4).

Given the analytical form of the Mach number (15), the Rankine–Hugoniot relations can be used to write a simple expression for the peak hydrostatic overpressure behind the shock front as

$$\Delta P=\frac{7P_0}{6}\left(M_S^2-1\right)=\frac{7P_0}{6K_0z^3}=\frac{7E_m}{6K_0}Z^{-3}, \tag{21}$$

where the last form is relevant for chemical explosions. The energy of the explosion has been related to the mass of a charge by $E_0=E_mW$, where E_m is the specific energy per unit mass that characterizes the chemical energy con-

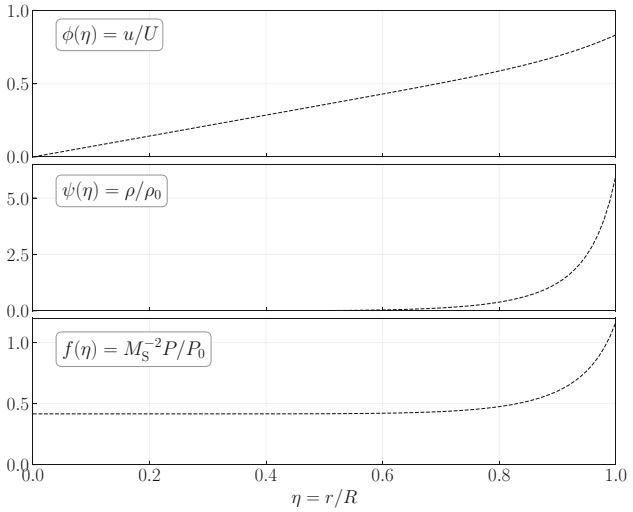

Fig. 1 Solutions of the hydrodynamics equations as functions of the dimensionless radial coordinate η

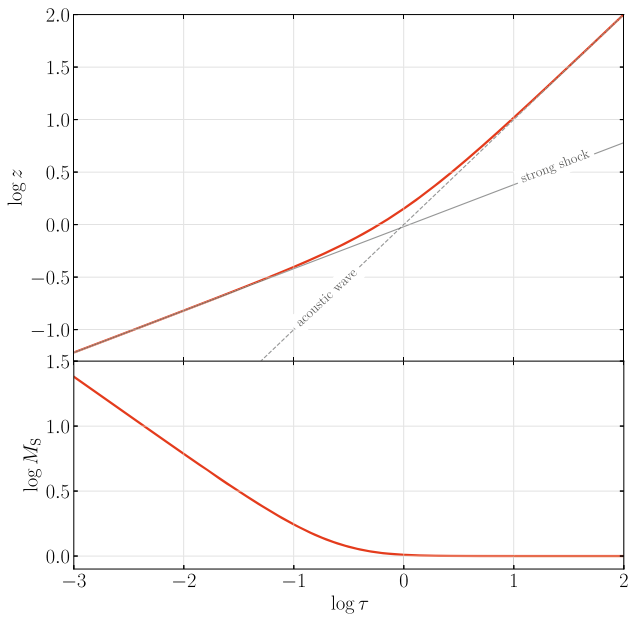

Fig. 2 Blast wave solutions: the solution of (15) smoothly transitions from the strong-shock limit to the acoustic regime characterizing the decay of the blast wave to an acoustic wave. Bottom: analytical expression for the shock's Mach number decreasing by several orders of magnitude

verted into kinetic and thermal energy after the explosion. For example, considering a TNT explosion ($E_m \approx 4.3$ MJ/kg) the oversimplified expression (21) leads to an overpressure barely distinguishable from the Brode formula for spherical blasts [12]. Being an approximation, the overpressure (21) captures only some of the features of its decay with distance. The absence of the logarithmic dependency with distance is a sign of a deviation from other standard description of the blast wave in the far field [3,4,49,50].

3 Sedov–Taylor–von Neumann Blast Wave

The well-known Sedov–Taylor–von Neumann (STvN) solution [7–9], also known as the strong-shock limit, assumes an intense explosion so that the ambient pressure of the undisturbed gas P_0 is negligible compared to the pressure behind the shock front. Both Taylor and von Neumann studied spherical explosions, whereas Sedov obtained a more general solution applicable to other geometries. Here we only focus on the spherical case for an instantaneous release of the explosive energy. This limit corresponds to $\lambda \to 0$ and neglects the thermal energy of the gas before the explosion. This is equivalent to solving the blast wave equation (15) for the early stages of the explosion when $z^3 \ll K_0^{-1}$, simplifying the Mach number equation to the reduced form

$$M_S(z) = \frac{\mathrm{d}z}{\mathrm{d}\tau} \approx K_0^{-1/2} z^{-3/2}, \tag{22}$$

whose solution is

$$z(\tau) = \left(\frac{25}{4K_0}\right)^{1/5} \tau^{2/5}, \tag{23}$$

shown in Fig. 2 as a straight line of slope 2/5 in the log-log plane. In standard coordinates, we recover the more familiar form

$$\frac{\mathrm{d}R}{\mathrm{d}t} = \left(\frac{\gamma E_0}{K_0 \rho_0}\right)^{1/2} R^{-3/2}, \tag{24}$$

whose solution is the well-known STvN blast wave

$$R = \left(\frac{25\gamma}{4K_0}\right)^{1/5} \left(\frac{E_0 t^2}{\rho_0}\right)^{1/5}. \tag{25}$$

The constant factor for air is

$$S(\gamma) = \left(\frac{25\gamma}{4K_0}\right)^{1/5} = 1.022, \tag{26}$$

which is moderately closer to the exact value $S(1.4) = 1.033$ than the approximate result $S(1.4) = 1.014$ found by Chernyi [17]. It should be emphasized that this description of a blast wave is only valid in the early stages of expansion and where the explosion can be assumed to originate as point-source energy release, such as a nuclear explosion or in the mid-range for a chemical explosion. In a later stage, a blast wave will decay and the strong-shock approximation will no longer be valid (and in the early stages of a chemical explosion the energy release will not be from a point-source). For a full description of the blast wave, and more crucially, including the transition from a strong shock to an acoustic wave we must solve the equation for the general Mach number (15).

As shown in (22), the STvN solution is obtained when neglecting the thermal energy of the undisturbed air before the explosion via the strong-shock condition ($P \gg P_0$). Similarly, by comparing the general differential equation (15) describing the blast wave and the STvN limit (22), we can write an upper value for the validity of the STvN solution from the general expression (15) in the form

$$z_{\mathrm{upp}} \lesssim K_0^{-1/3} = 0.50. \tag{27}$$

For scaled distances higher than z_{upp}, deviations from the STvN solution are expected due to the decay of the shock wave. This behavior is independent of the type of explosion: chemical or nuclear.

In the other direction, there is also a lower value z_{low} for the range of validity of the STvN solution for chemical explosions. The solution neglects the mass of the explosive charge W compared to the mass of the surrounding air over which energy has to be transferred. For this reason, there is a minimum distance from the center of the explosion where the mass of the charge can no longer be neglected. Imposing the condition $m_{\mathrm{air}} \gtrsim 2W$, we find

$$\left(\frac{3P_0}{2\pi\rho_0 E_m}\right)^{1/3} \lesssim z_{\mathrm{low}}, \tag{28}$$

where E_m is the specific energy per unit mass introduced in the previous section. In standard dimensions, the range of validity of the STvN solution can be written in the form

$$\left(\frac{3W}{2\pi\rho_0}\right)^{1/3} < R < \left(\frac{E_m W}{K_0 P_0}\right)^{1/3}. \tag{29}$$

Using scaled distance $Z = R/W^{1/3}$, the range of validity of the STvN solution in air becomes

$$0.73\ \mathrm{m/kg^{1/3}} < Z < \left(1.3\, E_m\right)^{1/3}\ \mathrm{m/kg^{1/3}}, \tag{30}$$

where the specific energy per unit mass E_m must be in MJ/kg. This range is consistent with the experimental results

Table 1 Range of validity of the STvN solution for some explosives

	TNT	PE4/C4	AN
E_m (MJ/kg)	4.294	5.621	1.447
z_{low}	0.21	0.19	0.30
z_{upp}	0.50	0.50	0.50
Z_{low} (m/kg$^{1/3}$)	0.73	0.73	0.73
Z_{upp} (m/kg$^{1/3}$)	1.77	1.94	1.23

Values of E_m from [18,19]

presented in [7]. Explicit values for TNT, PE4, and ammonium nitrate are presented in Table 1.

4 Experiments

As mentioned in the previous section, a useful property of the dimensionless scaled coordinates (τ, z) is that we can visualize explosions from multiple different yields in a single plot. In this section, we consider measurements of the arrival time of the shock front at different distances for a variety of explosions and show how these measurements agree with the analytical results from the previous sections. For nuclear explosions, the units kt and Mt refer to 10^3 and 10^6 tonnes of TNTe, respectively. Note that in all cases E_0 is determined in joules and the relation 1 kt = 4.18 TJ is subsequently used to convert units.

4.1 Early nuclear explosions

From the first nuclear test (Trinity), nuclear explosions with yields in the dozens of kilotons were abundant during the late 1940s through the 1950s. Many unclassified technical reports of these tests include information of the pressure measurements at different distances from ground zero [33,34]. In particular, Trinity is the only test for which early data is available and this is in fact what G.I. Taylor used in his second paper [35]; however, the far-field data is missing. General Leslie Groves requested many first-hand accounts describing the reactions of people who witnessed the Trinity test [36]. These accounts include information of the writer's location and arrival time of the blast wave, which we have used to map the evolution of the Trinity blast in the far-field region shown in Fig. 3.

For all later nuclear tests, only mid- to far-field data are available, whereas early-time measurements at millisecond scales remain unpublished. A team of scientists, historians, and filmmakers at Los Alamos and Livermore National Laboratories are currently working on the restoration and digitization of old nuclear-tests films and it is expected that fireball data will be published in the near future.

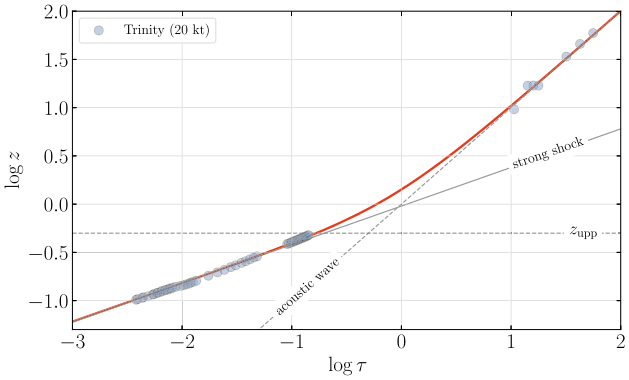

Fig. 3 Blast wave data of the Trinity test. As described by Taylor [35], the fireball data follows the STvN solution. The measurements reported by witnesses of the test from different locations follow the curve in the acoustic regime

4.2 Gram-sized explosive charges

The explosion of gram-sized charges offers the possibility of studying the very early stages of a blast as well as the influence of different charge geometries. High-speed cameras allow for recording of the early shock wave and pressure gauges can measure overpressure histories from which arrival time can be determined. In recent years, researchers at the University of Sheffield (UoS) Blast and Impact Laboratory have conducted approximately 80 far-field arena tests using hemispheres of PE4 explosive [20–24], and a smaller number of near-field tests using spheres of PE4 [25,26]. The results are shown in the top-left panel of Fig. 4. For comparison, the figure also includes the curve of the ConWep data for 1 kg of TNT [27]. One important observation to make is that in deriving the blast wave (15) the explosive is considered a point source and the energy is released within an infinitesimally small volume. For nuclear explosions, this approximation is valid; however, it breaks down in the near field of chemical explosions because the size of the explosive charge cannot be neglected. For this reason, the solution of (15) fails to properly capture the close-in behavior of chemical explosions and the semi-empirical ConWep curve works better, as shown in Fig. 4.

4.3 Large chemical explosions

Many tests of significant amounts of explosives have been carried out using TNT and ANFO to mimic the effects of kiloton-range nuclear explosions [28,29]. Accidental explosions, such as the Beirut blast [30–32], also allow for studies in this range. The data for a selection of explosions in this range are shown in the top-right panel of Fig. 4. Similar to small explosive charges, in the near field the ConWep curve works better than the solution of (15).

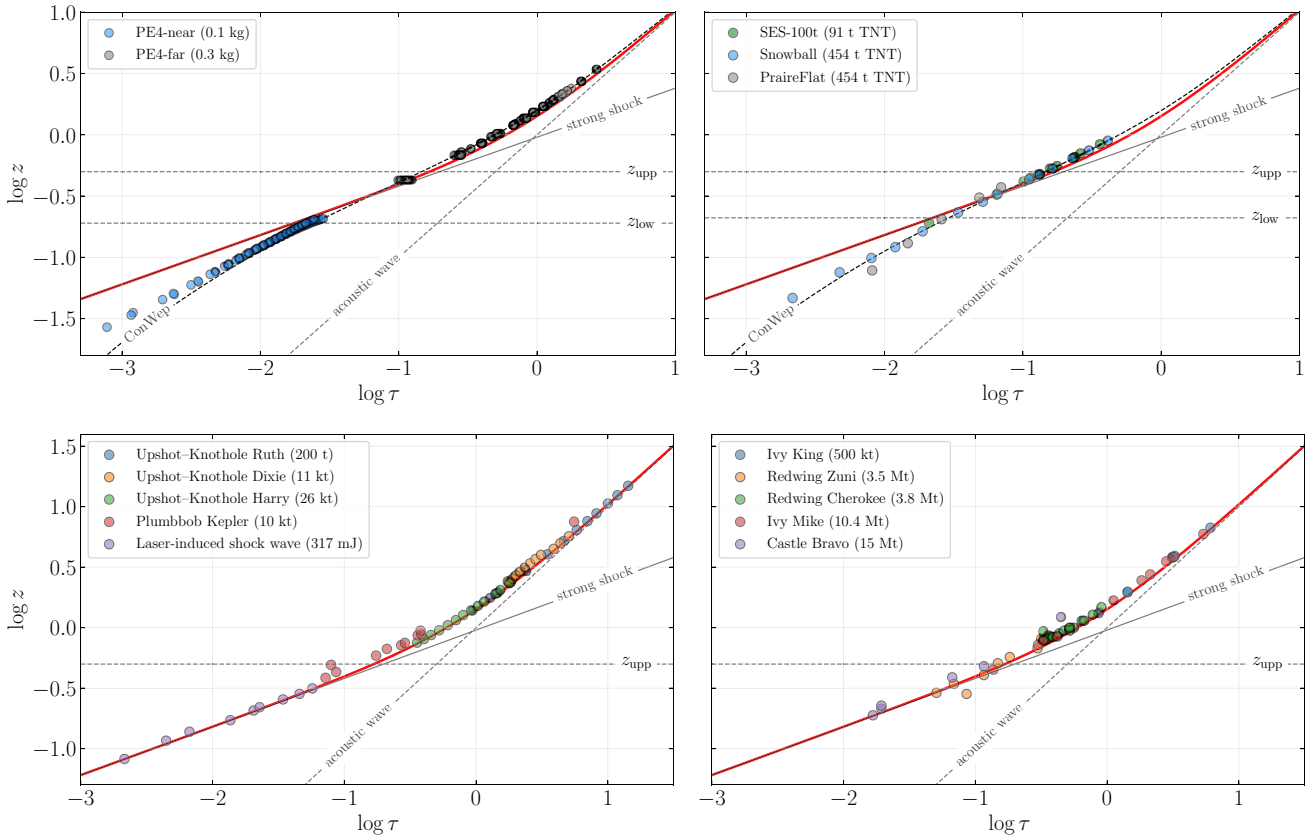

Fig. 4 Top: Blast wave data from a collection of gram-sized charges (left) and large chemical explosions (right). The upper and lower limits for the validity of the STvN solutions are indicated and the curve of the ConWep data for 1 kg of TNT is also shown. Bottom: Blast wave data from a collection of early nuclear tests and from laser-induced shock waves (left); and data from some historical thermonuclear tests (right)

4.4 Laser-induced shock waves

Shock waves can be generated by the fast deposition of energy in different materials by laser pulses. A second laser can be used for diagnostics of the produced plasma, and some of its properties can be inferred by studying the time evolution of the shock as well as the plasma plume in a variety of geometries. These laser-induced shocks are usually characterized by the STvN solution [37]. Data of a spherical shock produced by a joule-range laser are included in the bottom-left panel of Fig. 4.

4.5 Thermonuclear explosions

During the Cold War, the development of advanced nuclear weapons pushed the yield from kilotons to megaton thermonuclear tests [38–40]. The formidable amount of energy released by these explosions allows for reliable measurements only very far from ground zero; however, the high yields lead to short-scaled distances and times into the mid-field region. Results from a selection of thermonuclear test are shown in Fig. 4. Note that in this figure, error bars are either not available or are indistinguishable at this scale.

5 Applications

One useful application of the results of the previous sections is the determination of the yield, E_0, of an explosion from a set of (t, R) pairs. It is tempting to simply fit the solution of (15) to data; nonetheless, there are a few considerations to keep in mind to avoid falling into conceptual traps:

1. One aspect to take into account is the behavior of the curve at different ranges. As shown in Fig. 2, the solution coincides with the STvN line in the short range, meaning that for very early times and short distances the solution might fail to properly describe a chemical explosion; this is not an issue for nuclear explosions, as mentioned in Sect. 3.
2. Additionally, the solution in the long range asymptotically approaches the acoustic wave ($M_S \to 1$) independent of the energy E_0. This feature translates into a highly

degenerate solution, making the use of long-range-only data unreliable for determining E_0. This degeneracy is broken in the short range, and for this reason short-range data are crucial for a reliable determination of E_0.

3. Fitting the solution of (15) to data in the (t, R) space makes the analysis highly sensitive to the values of the long-range data, where large uncertainties can render the analysis useless. Furthermore, the breaking of degeneracy described in the previous point is negligible on a linear scale. Instead, the fit ought to be carried out in the $(\log \tau, \log z)$ space, where the log-log scale eliminates the problems from the linear scale.
4. A consequence of using the $(\log \tau, \log z)$ space for the fit is that the individual uncertainties (measured in the (t, R) space) become large in the short range and small in the long range.

As an illustrative example, let us consider the dataset of (t, R) pairs from the Beirut explosion [31,32] and use the results from Sect. 2 to estimate the yield that caused this blast. We can relate the physical quantities t and R to the dimensionless variables τ and z using the unknown parameter E_0 and then minimize a loss function with respect to the numerical solution of (15). A robust method is obtained by using `emcee`, a Python implementation of the affine-invariant ensemble sampler for Markov chain Monte Carlo (MCMC) [41,42]. Using the combined datasets from Refs. [31,32], the resulting posterior probability distribution of the model parameter E_0 is shown in Fig. 5. The value $E_0 = 514^{+41}_{-43}$ tonne TNTe represents the median of the distribution, and the uncertainties are based on the 16th and 84th percentiles of the sample.

This value accounts for the fact that the Beirut explosion took place at ground level rather than in free air (assumed in previous sections). The correction is obtained by dividing E_0 by the reflection factor to account for the enhancement of the shock wave due to the ground-reflected hemisphere and the

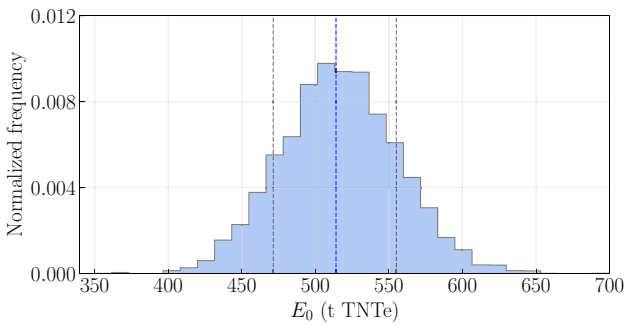

Fig. 5 Posterior probability distribution of the model parameter E_0. The value $E_0 = 514^{+41}_{-43}$ tonne TNTe represents the median of the distribution and the uncertainties are based on the 16th and 84th percentiles of the sample, shown in the plot

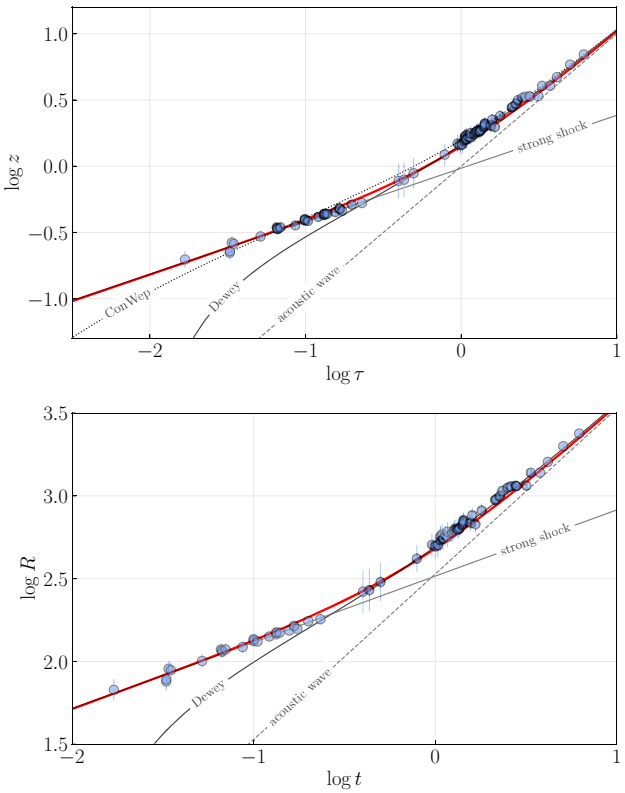

Fig. 6 Data from the Beirut explosion; the value $E_0 = 514$ tonne TNTe was used for scaling the data (top) in the dimensionless coordinates (τ, z) and the blast wave curve (bottom) in standard coordinates (t, R)

energy loss due to cratering and ground shock. In this study, we deem a reflection factor of 1.8 to be most suitable [43], due to ground conditions and the built-up nature of the Port of Beirut and its surroundings. For explosions near sea level, during nuclear tests on the Pacific Proving Grounds it was found that the reflection factor is closer to 1.6 due to extra energy dissipation in the form of large water displacements [44]. Indeed, the reflection factor is known to be a function of radius, ranging from as low as 1.26 and asymptotically approaching 2.0 at very large distances. The analyst is free to use any reflection factor they deem suitable.

Figure 6 shows the data and the corresponding scaling using the value $E_0 = 514$ tonne TNTe. Note that the first plot shows the $(\log \tau, \log z)$ space so the curves are scale independent, whereas the data are scaled. On the contrary, the second plot shows the $(\log t, \log R)$ space, in which the curves rather than the data are scaled. For comparison, in the same figure the curve of the ConWep data for 1 kg of TNT has also been included (top panel) as well as the Dewey fit for this particular explosion [45]. Dewey's fit properly describes the data after the shock speed drops below Mach 2; moreover, it exhibits the logarithmic decay into the acoustic limit that (15) does not capture. As a trade off, the shock described by (15) is generic and it corresponds to a unique solution

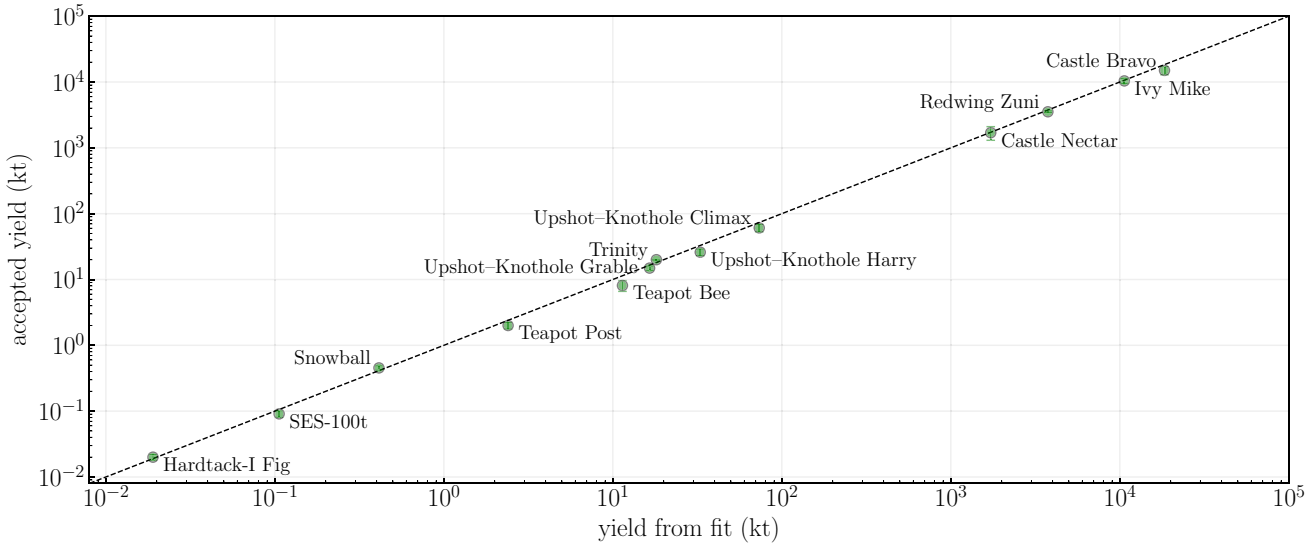

Fig. 7 Comparison between fitted and accepted yield E_0 for thirteen explosions over a wide range of energies shown in kilotons

valid for any explosion, whereas Dewey's approach requires fitting the free parameters for each explosion individually. Additionally, (15) is valid over the whole transition range from the strong shock to the acoustic limit.

The value of E_0 found above is in excellent agreement with other yield determinations of the Beirut explosion, including those performed independently by each of the present authors [31,32] and others. As a more general validation of the method, we have applied it for estimating the yield of a selection of high-explosives and nuclear tests over a wide range of energies, from a few tonnes of TNTe to the high yields of thermonuclear tests [28,33,34,38–40,46–48]. The results of the fit of E_0 for thirteen historical explosions are shown in Fig. 7, where the fits are compared to the "accepted" yield in tonnes of TNTe (since the "true" yield may not be known). As indicated earlier, the accuracy of the parameter fit relies on the availability of data in the early stages. Similarly, the precision of the parameter fit depends on the noise level of the dataset. These features are noticeable in the figure for the noisiest datasets corresponding to the tests Bee (Operation Teapot) and Harry (Operation Upshot-Knothole).

The excellent agreement between the fitted and accepted yields over several orders of magnitude confirms that (15) provides an acceptable description of the shock front, despite the unrefined approximation of a linear decay of the Mach number. We remark in passing that an evident deviation from the exact description of the Mach number appears as the decay into the acoustic regime according to (15) does not include the logarithmic dependency found both theoretically [49] and semi-empirically [50].

6 Summary and conclusions

This article illustrates the results of a general characterization of a blast wave in free air, extendable to other configurations by using a reflection factor. A linear ansatz for the decay of the Mach number of the shock front as it expands allows for analytical solutions of the hydrodynamics equations that lead to a concise expression for the Mach number of shock front in terms of the distance from the explosion center. Despite the unsophisticated approximation for the deceleration of the shock front, the subsequently obtained expressions show an excellent agreement with experimental data.

A simple formula for the Mach number was derived in the form of an ordinary differential equation, whose solution describes the position versus time development of the shock front. Here is where time of arrival measurements can be used for estimating the energy E_0 producing the shock wave, a crucial parameter that determines the shock evolution and the loading developed on obstacles with which it interacts. The general solution found contains the well-known strong-shock solution as a limit in the early stage of the shock development, beyond this regime the solution describes the transition to an acoustic wave in the far-field. In the near field, the solution is only valid for nuclear explosions because a point source was assumed. Experimental data from gram-sized charges were used to verify the validity of the results and later archival data from large-scale explosions were also employed using dimensionless coordinates for time and distance so that explosions from grams of PE4 to thermonuclear blasts can be visualized in a single diagram. The

solution found serves as a generalization of other descriptions of the decaying blast wave, in this case, valid from the early (strong) stage to the asymptotically acoustic behavior at the far field. In a similar fashion, an interesting new scaling to dimensionless coordinates has been recently proposed that allows visualizing explosions in air and underwater in the same plot [51].

A discussion about the validity of the strong-shock solution was presented that can serve a valuable resource for blast engineers. The yields of over a dozen explosions were estimated as way to validate the results found in this work and the main aspects of a fit to time-of-arrival data are discussed. Our results show that one of the key features when fitting the yield to time-of-arrival data is that this must be performed in a log-log space; otherwise, slight errors in far-field data will dramatically affect the estimate of E_0 and can possibly render the analysis useless. This property is due to the highly degenerate nature of the blast wave solution in the far field, where all solutions asymptotically approach to an acoustic wave independent of the yield E_0. Additionally, when applied to laser-induced shocks, the method outlined in this work becomes a direct diagnostic of the laser energy deposited in the material.

Supplementary Information The online version contains supplementary material available at https://doi.org/10.1007/s00193-022-01089-z.

Acknowledgements J.S.D. was supported in part by the Indiana University Center for Spacetime Symmetries. He also acknowledges the delightful company of H. Fry and A. Rutherford with their *Curious Cases* during most of this work, and thanks J.C. Valenzuela for bringing laser-induced shock waves to our attention.

Declarations

Conflict of interest The authors declare that they have no conflict of interest.

References

1. Agapiou, A.: Damage proxy map of the Beirut explosion on 4th of August 2020 as observed from the Copernicus sensors. Sensors **20**(21), 6382, 1–21 (2020). https://doi.org/10.3390/s20216382
2. Norville, H.S., Harvill, N., Conrath, E.J., Shariat, S., Mallonee, S.: Glass-related injuries in Oklahoma City bombing. J. Perform. Constr. Fac. **13**(2), 50–56 (1999). https://doi.org/10.1061/(ASCE)0887-3828(1999)13:2(50)
3. Dewey, J.M.: The air velocity in blast waves from T.N.T. explosions. Proc. R. Soc. Lond. **A279**, 366–385 (1964). https://doi.org/10.1098/rspa.1964.0110
4. Dewey, J.M.: The properties of a blast wave obtained from an analysis of the particle trajectories. Proc. R. Soc. Lond. **A324**, 275–299 (1971). https://doi.org/10.1098/rspa.1971.0140
5. Dewey, J.M.: The Rankine–Hugoniot equations: their extensions and inversions related to blast waves. Sochet, I. (ed.) Blast Effects: Physical Properties of Shock Waves, Chapt. 2. Springer Nature (2018). https://doi.org/10.1007/978-3-319-70831-7
6. Gallet, A., Rigby, S.E., Tallman, T.N., Kong, X., Hajirasouliha, I., Liew, A., Liu, D., Chen, L., Hauptmann, A., Smyl, D.: Structural engineering from an inverse problems perspective. Proc. R. Soc. Lond. **A478**, 20210526 (2022). https://doi.org/10.1098/rspa.2021.0526
7. Taylor, G.I.: The formation of a blast wave by a very intense explosion, I: theoretical discussion. Proc. R. Soc. Lond. **A201**, 159–174 (1950). https://doi.org/10.1098/rspa.1950.0049
8. Sedov, L.I.: Similarity and Dimensional Methods in Mechanics. Academic Press, New York (1957). https://doi.org/10.1016/C2013-0-08173-X
9. von Neumann, J.: Collected Works, vol. 6. Pergamon, New York (1963). https://doi.org/10.2307/2003380
10. Sakurai, A.: On the propagation and structure of the blast wave. I. J. Phys. Soc. Jpn. **8**, 662–669 (1953). https://doi.org/10.1143/JPSJ.8.662
11. Sakurai, A.: On the propagation and structure of the blast wave. II. J. Phys. Soc. Jpn. **9**, 256–266 (1954). https://doi.org/10.1143/JPSJ.9.256
12. Brode, H.L.: Numerical solution of spherical blast waves. J. Appl. Phys. **26**, 766–775 (1955). https://doi.org/10.1063/1.1722085
13. Brode, H.L.: Blast wave from a spherical charge. Phys. Fluids **2**, 217–229 (1955). https://doi.org/10.1063/1.1705911
14. Brode, H.L.: Fireball Phenomenology. RAND Corporation, Santa Monica (1964). https://www.rand.org/pubs/papers/P3026.html
15. Bach, G.G., Lee, J.H.S.: An analytical solution for blast waves. AIAA J. **8**, 271–275 (1970). https://doi.org/10.2514/3.5655
16. Baker, W.E., Westine, P.S., Dodge, F.T.: Similarity methods in engineering dynamics: theory and practice of scale modeling. Spartan Books (1973). https://doi.org/10.1016/c2009-0-12656-9
17. Zel'dovich, Y.B., Raizer, Y.P.: Physics of Shock Waves and High-Temperature Hydrodynamic Phenomena. Dover Books on Physics, New York (1967). https://doi.org/10.1016/b978-0-12-395672-9.x5001-2
18. Dobratz, B.M.: LLNL explosives handbook—properties of chemical explosives and explosive stimulants. Technical Report UCRL-51319, LLNL, University of California, CA, USA (1972). https://doi.org/10.2172/4285272
19. Oommen, C., Jain, S.R.: Ammonium nitrate: a promising rocket propellant oxidizer. J. Hazard. Mater. **67**(3), 253–281 (1999). https://doi.org/10.1016/S0304-3894(99)00039-4
20. Rigby, S.E., Tyas, A., Bennett, T., Clarke, S.D., Fay, S.D.: The negative phase of the blast load. Int. J. Prot. Struct. **5**(1), 1–20 (2014). https://doi.org/10.1260/2041-4196.5.1.1
21. Rigby, S.E., Fay, S.D., Tyas, A., Warren, J.A., Clarke, S.D.: Angle of incidence effects on far-field positive and negative phase blast

parameters. Int. J. Prot. Struct. **6**(1), 23–42 (2015). https://doi.org/10.1260/2041-4196.6.1.23
22. Tyas, A., Warren, J., Bennett, T., Fay, S.: Prediction of clearing effects in far-field blast loading of finite targets. Shock Waves **21**(2), 111–119 (2011). https://doi.org/10.1007/s00193-011-0308-0
23. Tyas, A.: Blast loading from high explosive detonation: what we know and what we don't know. 13th International Conference on Shock and Impact Loads on Structures, Guangzhou, China (2019)
24. Rigby, S.E., Tyas, A., Fay, S.D., Clarke, S.D., Warren, J.A.: Validation of semi-empirical blast pressure predictions for far field explosions: Is there inherent variability in blast wave parameters? 6th International Conference on Protection of Structures Against Hazards (PSH14), 16–17 October, Tianjin, China (2014)
25. Rigby, S.E., Tyas, A., Clarke, S.D., Fay, S.D., Reay, J.J., Warren, J.A., Gant, M., Elgy, I.: Observations from preliminary experiments on spatial and temporal pressure measurements from near-field free air explosions. Int. J. Prot. Struct. **6**(2), 175–190 (2015). https://doi.org/10.1260/2041-4196.6.2.175
26. Rigby, S.E., Knighton, R., Clarke, S.D., Tyas, A.: Reflected near-field blast pressure measurements using high speed video. Exp. Mech. **60**(7), 875–888 (2020). https://doi.org/10.1007/s11340-020-00615-3
27. Hyde, D.W.: Conventional Weapons Program (ConWep), U.S. Army Waterways Experimental Station, Vicksburg, MS, USA
28. Reisler, R.E., Keefer, J.H., Giglio-Tos, L.: Basic air blast measurements from a 500-ton TNT detonation, Project 1.1, Operation Snowball. Ballistic Research Laboratories, Report No. 1818 (1966). https://apps.dtic.mil/sti/citations/AD0814989
29. Murrell, D.W.: Earth motion and stress measurements. Operation Prairie Flat, Project LN302, U.S. Army Engineer Waterways Experiment Station (1972). https://www.osti.gov/biblio/4665747
30. Pilger, C., Gaebler, P., Hupe, P., Kalia, A.C., Schneider, F.M., Steinberg, A., Sudhaus, H., Ceranna, L.: Yield estimation of the 2020 Beirut explosion using open access waveform and remote sensing data. Sci. Rep. **11**, 14144 (2021). https://doi.org/10.1038/s41598-021-93690-y
31. Rigby, S.E., Lodge, T.J., Alotaibi, S., Barr, A.D., Clarke, S.D., Langdon, G.S., Tyas, A.: Preliminary yield estimation of the 2020 Beirut explosion using video footage from social media. Shock Waves **30**, 671–675 (2020). https://doi.org/10.1007/s00193-020-00970-z
32. Díaz, J.S.: Explosion analysis from images: Trinity and Beirut. Eur. J. Phys. **42**, 035803 (2021). https://doi.org/10.1088/1361-6404/abe131
33. Swift, L.M., Sachs, D.C.: Air pressure and ground shock measurements, Operation Upshot-Knothole, Project 1.1b. Stanford Research Institute, WT-711 (1953). https://apps.dtic.mil/sti/citations/AD0373321
34. Swift, L.M., Sachs, D.C., Kriebel, A.R.: Airblast phenomena in the high pressure region (U). Operation Plumbbob, Project 1.3. Stanford Research Institute, WT-1403 (1957). https://apps.dtic.mil/sti/citations/AD0611257
35. Taylor, G.I.: The formation of a blast wave by a very intense explosion, II: the atomic explosion of 1945. Proc. R. Soc. Lond. **A201**, 175–186 (1950). https://doi.org/10.1098/rspa.1950.0050
36. Dannen, G.: Trinity. U.S. National Archives, Record Group 227, OSRD-S1 Committee, Box 82 folder 6. http://www.dannen.com/decision/trin-eye.html (1995). Accessed 17 April 2021
37. Gatti, M., Palleschi, V., Salvetti, S., Vaselli, M.: Spherical shock waves in laser produced plasmas in gas. Opt. Commun. **69**, 141–146 (1988). https://doi.org/10.1016/0030-4018(88)90299-4
38. Haskell, N.A., Vann, J.O., Gast, P.R.: Free-air atomic blast pressure and thermal measurements. Operation Ivy Project 6.11, WT-361 (1952). https://apps.dtic.mil/sti/citations/AD0363575
39. Kingery, C.N., Hoover, C.H., Keefer, J.H.: Ground surface air blast pressure vs distance (U). Operation Redwing, Project 1.1, Ballistic Research Laboratories, WT-1301 (1956). https://apps.dtic.mil/sti/citations/ADA995110
40. Meszaros, J.J., Kingery, C.N.: Ground surface air pressure vs distance from high-yield detonations (U), Operation Castle, Project 1.2b. Ballistic Research Laboratories, WT-905 (1957). https://www.osti.gov/biblio/6032132
41. Foreman-Mackey, D., Hogg, D.W., Lang, D., Goodman, J.: Emcee: the MCMC Hammer. PASP **125**(925), 306–312 (2013). https://doi.org/10.1086/670067
42. Goodman, J., Weare, J.: Ensemble samplers with affine invariance. Commun. Appl. Math. Comput. Sci. **5**, 65–80 (2010). https://doi.org/10.2140/camcos.2010.5.65
43. Smith. P., Cormie, D.: Blast loading. In: Cormie, D., Mays, G., Smith, P. (eds.) Blast Effects on Buildings, 2nd edn. ICE Publishing (2009). https://doi.org/10.1680/beob2e.35218.0003
44. Coleman, K.D., Higgs, A.H., Killion, L.E., Bingham, H.T., Kelso, J.R., Facer, G.C., Chiment, J.A., Van Lint, V.A.J., Clarke, J.F., Bankes, C.W., O'Brien, F.E., Shilling, S.G., Black, H., Linton, W.C., James, J.G., Sheahan, W.M., Isengard, W.S., Forsyth, G.P., Williams, P.W., Miller, W.J., Jennings, E.R., McNeill, D.A.: Operation Castle: Summary report of Military Effects, Task Unit 13, Programs 1-9 (1954). https://www.osti.gov/opennet/servlets/purl/16039007
45. Dewey, J.M.: The TNT and ANFO equivalences of the Beirut explosion. Shock Waves **31**, 95–99 (2021). https://doi.org/10.1007/s00193-021-00992-1
46. Kingery, C.N., Keefer, J.H., Day, J.D.: Surface air blast measurements from a 100-ton TNT detonation. Ballistic Research Laboratories, Report No. 1410 (1962). https://apps.dtic.mil/sti/citations/AD0285599
47. Technical summary of Military Effects Programs 1–9, Sanitized Version, Operation Hardtack preliminary report ITR-1660-(SAN) (1959). https://apps.dtic.mil/sti/citations/ADA369152
48. Sachs, D.C., Swift, L.M., Sauer, F.M.: Air blast overpressure and dynamic pressure over various surfaces. Operation Teapot, Project 1.10, Stanford Research Institute, WT-1109 (1955). https://www.osti.gov/biblio/4828931
49. Bethe, H., Fuchs, K., Hirschfelder, J.O, Magee, J.L., Peierls, R.E., von Neumann, J.: Blast Wave. Los Alamos Scientific Laboratory, Technical Report LA-2000 (1958). https://apps.dtic.mil/sti/citations/ADA384954
50. Dewey, J.M.: Measurement of the physical properties of blast waves. In: Igra, O., Seiler, F. (eds.) Experimental Methods of Shock Wave Research. Springer, Cham, pp. 53–86 (2016). https://doi.org/10.1007/978-3-319-23745-9
51. Wei, T., Hargather, M.J.: A new blast wave scaling. Shock Waves **31**, 231–238 (2021). https://doi.org/10.1007/s00193-021-01012-y